Mathematical Foundations of Data Sciences

Gabriel Peyré
CNRS & DMA
École Normale Supérieure
gabriel.peyre@ens.fr
www.gpeyre.com
www.numerical-tours.com

November 15, 2017

Chapter 15

Compressed Sensing

This chapter details an important class of inverse problems, which corresponds to using "random" forward operators Φ. This is interesting from an applicative point of view since it allows to model a novel class of imaging devices which can potentially have improved resolution with respect to traditional operators (e.g. low-pass filters for usual cameras) when using in conjunction with sparse regularization technics. This is also interesting from a theoretical point of view, since the mathematical analysis becomes much simpler than with deterministic operators, and one can have good recovery and stability performances. Let us however stress that the "physical" creation of hardware that fulfils the theoretical hypothesis, in particular in medical imaging, is still largely open (put aside some restricted areas), although the theory gives many insightful design guides to improve imaging devices.

The main references for this chapter are [29, 23, 38].

15.1 Motivation and Potential Applications

15.1.1 Single Pixel Camera

In order to illustrate the exposition, we will discuss the "single pixel camera" prototype developed at Rice University [**?**], and which is illustrated by the figure 15.1 (left). It is an important research problem of developing a new class of cameras allowing to obtain both the sampling and the compression of the image. Instead of first sampling very finely (ie with very large Q) the analog signal $\tilde{f}$ to obtain a $f \in \mathbb{R}^Q$ image then compressing enormously (ie with M small) using (**??**), we would like to dispose directly of an economic representation $y \in \mathbb{R}^P$ of the image, with a budget P as close to M and such that one is able to "decompress" y to obtain a good approximation of the image f_0.

The "single-pixel" hardware performs the compressed sampling of an observed scene $\tilde{f}_0$ (the letter "R" in Figure 15.1), which is a continuous function indicating the amount of light $\tilde{f}_0(s)$ reaching each point $s \in \mathbb{R}^2$ of the focal plane of the camera. To do this, the light is focused against a set of Q micro-mirrors aligned on the focal plane. These micro-mirrors are not sensors. Unlike conventional sampling (described in Section **??**), they do not record any information, but they can each be positioned to reflect or absorb light. To obtain the complete sampling/compression process, one very quickly changes P times the configurations of the micro-mirrors. For $p = 1, \ldots, P$, one sets $\Phi_{p,q} \in \{0, 1\}$, depending on whether the micromirror at position q has been placed in the absorbing (0) or reflective (value 1) position at step p of the acquisition. The total light reflected at step p is then accumulated into a single sensor (hence the name "single pixel", in fact it is rather a "single sensor"), which achieves a linear sum of the reflected intensities to obtain the recorded $y_p \in \mathbb{R}$ value. In the end, if the light intensity arriving on the surface c_q of the mirror indexed by $f_q = \int_{c_q} \tilde{f}_0(s)\mathrm{d}s$ is denoted (as in the **??** section) as q, the equation that links the discrete image $f \in \mathbb{R}^Q$

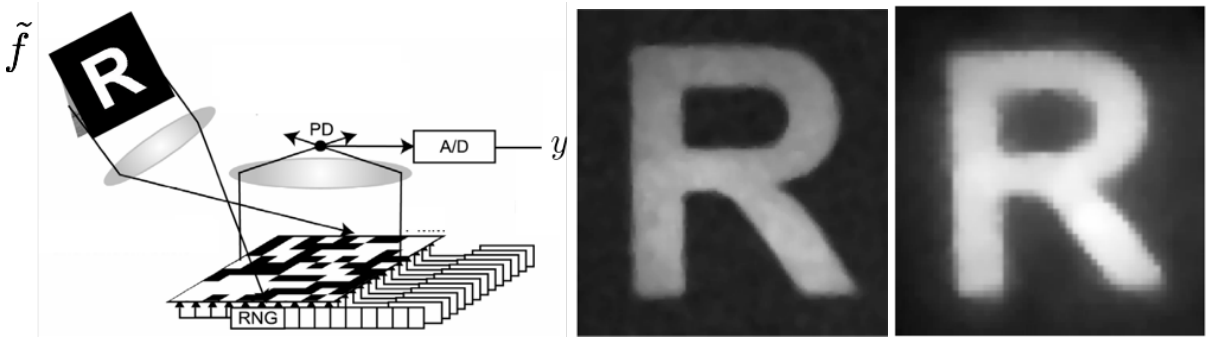

Diagram of the device f $f^\star$, $P/Q = 6$

Figure 15.1: Left: diagram of the single-pixel acquisition method. Center: image $f_0 \in \mathbb{R}^Q$ "ideal" observed in the focal plane of the micro-mirrors. Right: image $f_0^\star = \Psi x^\star$ reconstructed from observation $y \in \mathbb{R}^P$ with a compression factor $P/Q = 6$ using ℓ^1-type regularization.

"seen through the mirrors" to the P measures $y \in \mathbb{R}^P$ is

$$\forall\, p = 1, \ldots, P, \quad y_p \approx \sum_q \Phi_{p,n} \int_{c_n} \tilde{f}_0(s)\mathrm{d}s = (\Phi f_0)_p,$$

(here $\approx$ accounts for some noise), which corresponds to the usual forward model of inverse problems

$$y = \Phi f_0 + w \in \mathbb{R}^P$$

where w is the noise vector. It is important to note that the mirrors do not record anything, so in particular the f_0 discrete image is never calculated or recorded, since the device directly calculates the compressed representation y from the analog signal $\tilde{f}_0$. The term w models here the acquisition imperfections (measurement noise). The compressed sampling therefore corresponds to the transition from the observed scene $\tilde{f}_0$ to the compressed vector y. The "decompression" corresponds to the resolution of an inverse problem, whose goal is to find a good approximation of f_0 (the discrete image "ideal" as seen by the micro-mirrors) from y.

15.1.2 Sparse Recovery

In order to reconstruct an approximation of the (unknown) image f_0, following Section 11.2, we assume it is sparse in some dictionary Ψ. Denoting $A \overset{\text{def.}}{=} \Psi\Phi \in \mathbb{R}^{P\times N}$, this leads us to consider the usual ℓ^1 regularized poblem (11.10)

$$x_\lambda \in \operatorname*{argmin}_{x\in\mathbb{R}^Q} \frac{1}{2\lambda}\|y - Ax\|^2 + \|x\|_1, \tag{$\mathcal{P}_\lambda(y)$}$$

so that the reconstructed image is $f_\lambda = \Psi x_\lambda$. We also sometimes consider the constraint problem

$$x_\varepsilon \in \operatorname*{argmin}_{\|Ax-y\|\leqslant\varepsilon} \|x\|_1, \tag{$\mathcal{P}^\varepsilon(y)$}$$

where, for the sake of simplicity, we set $\varepsilon = \|w\|$ (which we assume is known). From a mathematical point of view, these problem are equivalent in the sense that there exists a bijection between λ and ε which links it solution. But in practice, this bijection is not explicitly known and depends on y.

Here, it is important to remember that A is drawn from a random matrix ensemble. For an arbitrary Ψ, it is hard to analyze this random distribution. If Ψ is orthogonal, and the distribution of the columns of Φ are invariant by rotation (which is the case if the entries are i.i.d. Gaussian), then A has the same distribution as Φ. In the following, we thus directly models the distribution of A and assumes it has some nice property (typically it is close to being Gaussian i.i.d.).

15.2 Dual Certificate Theory and Non-Uniform Guarantees

15.2.1 Random Projection of Polytopes

When there is no noise, $w = 0$ a way to tackle the problem is to use the caracterization of solutions of $(\mathcal{P}^0(Ax_0)) = (\mathcal{P}_0(Ax_0))$ given in Section 14.1.2. According to Proposition 43, identifiable vectors with sparsity $\|x_0\|_0 = s$ corresponds to s-dimensional faces of the ℓ^1 balls B_1 which are mapped to face of the projected polytope AB_1. This leads to a combinatorial problems to count the number of face of random polytope. Donoho and Tanner were able to perform a sharp analysis of this problem. They showed the existence of two regimes, using two functions C_A, C_M so that, with high probability (i.e. a probability converging exponentially fast to 1 with (n, p)) on the matrix A

– All x_0 so that $\|x_0\|_0 \leqslant C_A(P/N)P$ are identifiable.

– Most x_0 so that $\|x_0\|_0 \leqslant C_M(P/N)P$ are identifiable.

For instance, they show that $C_A(1/4) = 0.065$ and $C_M(1/4) = 0.25$. Figure 15.5 illustrates numerically these two phase transitions. This analysis can be shown to be sharp in high dimension, i.e. when $\|x_0\|_0 > C_M(P/N)P$, then x_0 is not identifiable with high probability (this corresponds to a phase transition phenomena). For large dimensions (N, P), the scaling given by C_M describe very well what one observe in practice. For $P = N/4$ (compression of a factor 4), one retrieve in practice all vector with sparsity smaller than P/N. The function C_M can be computed numerically, and it can be shown to have a logarithmic grows $C_M(r) \sim \log(r)$ for small r. This suggests that for high compression regime, one recovers with ℓ^1 minimization almost all vector with a sparsity $\|x_0\|_0$ proportional (up to log factor) to the number of measurements P.

15.2.2 Random Matrices

The analysis of the performance ℓ^1 minimization to solve compressed sensing problem is made possible because of the very precise understanding of the distribution of the singular values of certain random ensemble let us illustrate this in the Gaussian case, which is the simplest, and is very illustrative.

An important part of the recovery proof relies on controlling the correlation matrix $A_I^* A_I$ of selected columns, and even more importantly, its inverse $(A_I A_I)^{-1}$. These random matrices are called Wishart matrices and inverse Wishart matrices. Such a matrix $B = A_I$ is of size (P, s) and is also drawn from the Gaussian ensemble. Fixing s and letting $P \to +\infty$, one has thanks to the low of large numbers $B^* B \to \mathrm{Id}_s$ almost surely. This is however not a very realistic setting, since in general, one hope to have s almost equal, up to log factor, to P.

Linear growth $P = s/\beta$. A quite extreme setting is when s grows proportionally to P, and impose $s/P = \beta$. In this case, the eigenvalues of $B^* B$ are, for large p, essentially contained in the interval $[\lambda_-, \lambda_+]$ where $\lambda_\pm = (1 \pm \sqrt{\beta})^2$, $\beta \overset{\text{def.}}{=} p/s$, in the sense that the probability distribution of eigenvalues converges (in the weak sense of measures) toward the Marcenko-Pastur law

$$\forall\, (u, v) \in \mathbb{R}_+^2, \quad \mathbb{P}(\mathrm{eig}(B^\top B) \in [u, v]) \overset{p \to +\infty}{\longrightarrow} \int_u^v f_\beta(\lambda) \mathrm{d}\lambda$$

where one fix the ratio $\beta = s/P$, and the Marcenko-Pastur law is

$$f_\beta(\lambda) \overset{\text{def.}}{=} \frac{1}{2\pi\beta\lambda} \sqrt{(\lambda - \lambda_-)_+ (\lambda_+ - \lambda)}\, 1_{[\lambda_-, \lambda_+]}(\lambda).$$

Figure (15.3) illustrates this convergence.

Super-linear grows $P = s \log(\ldots)$. In order to have a better concentration of the singular values of $A_I^* A_I$ around 1, one needs to have a slightly super-linear growth of P with s. In this setting one has that $A_I^* A_I$. In order to derive non-asymptotic (i.e. with explicit constants) results, one can use a celebrated

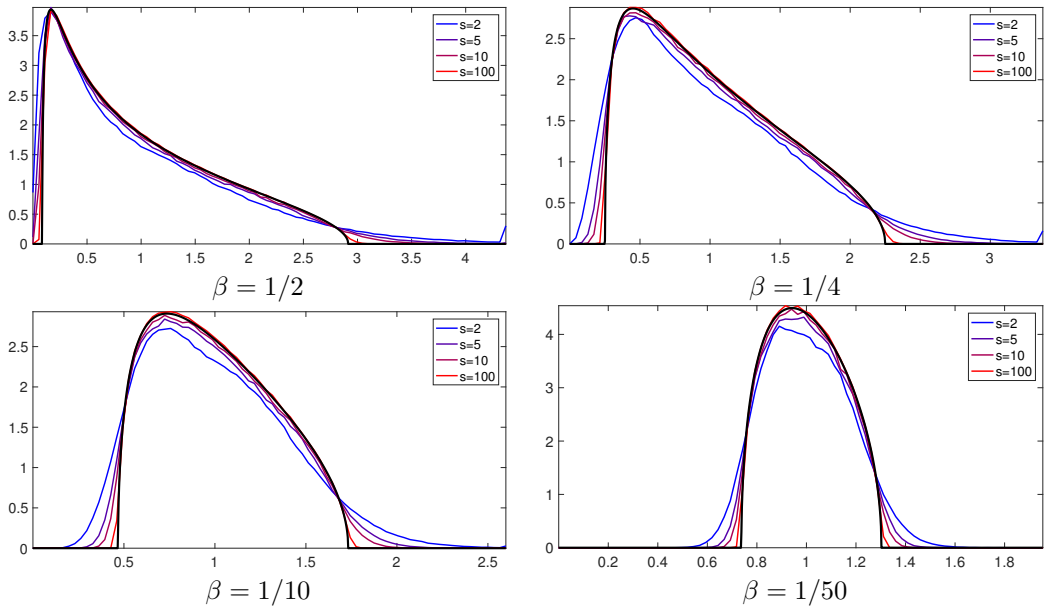

Figure 15.2: Illustration of the convergence toward the Marcenko-Pastur law.

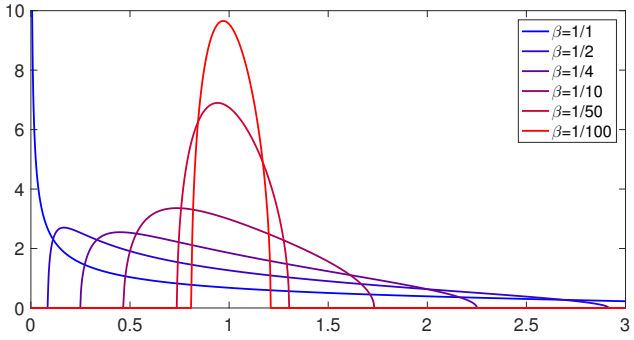

Figure 15.3: Display of the Marcenko-Pastur distribution f_β for various β.

concentration inequality due to Talagrand, which assert that one has a fast concentration of this randomized covariance $A_I^* A_I$ toward its expectation Id_s.

$$\mathbb{P}\left(\|A_I^* A_I - \mathrm{Id}_s\|_{\mathrm{op}} \geqslant t + \sqrt{\frac{s}{P}} \right) \leqslant e^{-\frac{t^2 s}{2}}. \tag{15.1}$$

15.2.3 Dual Certificates

In order to analyze recovery performance, one can looks not only for ℓ^2 stability ($\|x_\lambda - x_0\| \sim \|w\|$) but also that x_λ has the same support as x_0 when $\|w\|$ is small. As detailed in Section 14.2.3, this requires to ensure that the pre-certificate η_F defined in (14.24) is non-degenerated, i.e.

$$\|\eta_F\|_\infty \leqslant 1 \quad \text{where} \quad \eta_F = A^* A_I (A_I^* A_I)^{-1} \operatorname{sign}(x_{0,I}). \tag{15.2}$$

Figure 14.9 suggests that this should be the case if P is large enough with respect to $\|x_0\|$. This theorem backup this observation.

Coherence-based analysis. We first perform a crude analysis using the so-called coherence of the matrix $A = (a_j)_{j=1}^N$ where the $a_j \in \mathbb{R}^P$ are the columns of A, which we assume to be normalized $\|a_j\| = 1$

$$\mu \overset{\text{def.}}{=} \max_{0 \leqslant i \neq j} |\langle a_i, a_j \rangle| = \|A^* A - \mathrm{Id}_N\|_\infty \tag{15.3}$$

where $\|C\|_\infty = \max_{i,j} |C_{i,j}|$. The coherence is 0 for an orthogonal matrix, and is always larger than 1, $\mu \in [0,1]$. The smaller the coherence, the better conditioned the inverse problem $Ax = y$ is, and the more likely is the certificate η_F to be non-degenerate, as shown by the following proposition.

Proposition 51. *One has, denoting $s = \|x_0\|_0 = |I|$ where $I = \operatorname{supp}(x_0)$, for $\mu < \frac{1}{s-1}$,*

$$\|\eta_{F,I^c}\|_\infty \leqslant \frac{s\mu}{1-(s-1)\mu}. \tag{15.4}$$

In particular, if $s < \frac{1}{2}\left(1 + \frac{1}{\mu}\right)$, $\|\eta_{F,I^c}\|_\infty < 1$ and one can thus apply the recovery Theorem 44.

Proof. We recall that the ℓ^∞ operator norm (see Remark 8) is

$$\|B\|_\infty = \max_i \sum_j |B_{i,j}|.$$

We denote $C = A^* A$. One has

$$\|A_{I^c}^* A_I\|_\infty = \max_{j \in I^c} \sum_{i \in I} C_{i,j} \leqslant s\mu \quad \text{and} \quad \|\mathrm{Id}_s - A_I^* A_I\|_\infty = \max_{j \in I} \sum_{i \in I, i \neq j} C_{i,j} \leqslant (s-1)\mu$$

One also has

$$\begin{aligned} \|(A_I^* A_I)^{-1}\|_\infty &= \|((\mathrm{Id}_s - A_I^* A_I) - \mathrm{Id}_s)^{-1}\|_\infty = \|\sum_{k \geqslant 0} (\mathrm{Id}_s - A_I^* A_I)^k\|_\infty \\ &\leqslant \sum_{k \geqslant 0} \|\mathrm{Id}_s - A_I^* A_I\|_\infty^k \leqslant \sum_{k \geqslant 0} ((s-1)\mu)^k = \frac{1}{1-(s-1)\mu} \end{aligned}$$

which is legit because the matrix series indeed converge since $(s-1)\mu < 1$. Using these two bounds, one has

$$\|\eta_{F,I^c}\|_\infty = \|A_{I^c}^* A_I (A_I^* A_I)^{-1} \operatorname{sign}(x_{0,I})\|_\infty \leqslant \|A_{I^c}^* A_I\|_\infty \|(A_I^* A_I)^{-1}\|_\infty \|\operatorname{sign}(x_{0,I})\|_\infty \leqslant (s\mu) \times \frac{1}{1-(s-1)\mu} \times 1.$$

One has

$$\frac{s\mu}{1-(s-1)\mu} \quad \Longleftrightarrow \quad 2s\mu < 1 + \mu$$

which gives the last statement. □

Note that this proof actually shows that if $s < \frac{1}{2}\left(1+\frac{1}{\mu}\right)$, all certificate η_F are valid, for any sign pattern $\mathrm{sign}(x_0)$. This actually implies a much stronger stability in the sense that whatever the noise w (which might not be small), the support of x_λ is included (not necessarily equal) in the one of x_0.

One can show that one always has

$$\mu \geqslant \sqrt{\frac{N-P}{P(N-1)}}. \tag{15.5}$$

For Gaussian matrix $A \in \mathbb{R}^{P\times N}$, one has for large $(N,P) \to +\infty$

$$\mu \sim \sqrt{\log(PN)/P}$$

which shows that Gaussian matrix are close to being optimal for the bound (15.5) if $N \gg P$. Applying Proposition 51 thus shows that ℓ^1 regularization is able to recover with a stable support vector with less than $s \sim O(\sqrt{P})$ (ignoring log terms) non-zero coefficients. In face, we will show now that it does much better and recover a proportional number $s \sim O(P)$. This is because the coherence bound (15.4) is very pessimistic.

Randomized analysis of the Fuchs certificate. We consider here a class of sufficiently "random" matrices.

Definition 22 (sub-Gaussian random matrix)**.** *A random matrix $\sqrt{P}\,A$ is said to be sub-Gaussian if its entries are independent such that $\mathbb{E}(A_{i,j}) = 0$ (zero mean) $\mathbb{E}(A_{i,j}^2) = 1/P$ and*

$$\mathbb{P}(|\sqrt{P}\,A_{i,j}| \geqslant t) \leqslant \beta e^{-\kappa t^2}.$$

Note that its entries does not needs to be identically distributed, but the sub-Gaussiannity parameter (β,κ) should not depend on (i,j). Note also the presence of the normalization factor $\sqrt{P}$, which is here to ensure $\mathbb{E}(\|a_j\|^2) = 1$ where a_j are the columns of A.

Typical example of sub-Gaussian random matrix are Gaussian or Bernoulli matrices.

Theorem 45. *For a given $x_0 \in \mathbb{R}^N$, denoting $s = \|x_0\|_0$, and assuming A is sub-Gaussian, then for for any $0 < \varepsilon < 1$ provided that*

$$P \geqslant \frac{4c}{1-\delta} s \log(2N/\varepsilon) \quad \text{where} \quad \delta^2 \overset{\text{def.}}{=} \frac{C}{4c}\left(\frac{7}{\log(2N/\varepsilon)} + \frac{2}{s}\right)$$

condition (15.2) holds with probability $1-\varepsilon$, so that x_λ has the same support and sign as x_0 when $(\|w\|, \|w\|/\lambda)$ is small enough. The constant C, c, $C = \frac{2}{3\tilde{c}}$ where $\tilde{c} \overset{\text{def.}}{=} \frac{\kappa^2}{4\beta+2\kappa}$ only depends on the sub-Gaussianity parameter (β,κ) appearing (22), and for Gaussian or Benoulli matrices, $c = 1/2$.

Proof. We only give the main insight for the proof. Its crux relies on the fact that $\|A_{I^c}^* p_F\|_\infty \leqslant 1$ reads

$$\max_{j\notin I} |\langle a_j,\, p_F\rangle| \leqslant 1$$

where $p_F = A_I^{*+} s_{0,I}$ is *independent* from the vectors $(a_j)_{j\notin I}$ it is correlated against. This allows one to check this condition by first controlling $\|p_F\|$ and then making as if p_F was a fixed deterministic vector. Noticing

$$\|p_F\|^2 = \langle A_I(A_I^*A_I)^{-1}s_{0,I},\, A_I(A_I^*A_I)^{-1}s_{0,I}\rangle = \langle (A_I^*A_I)^{-1}s_{0,I},\, s_{0,I}\rangle,$$

the heuristic reasoning is that, following what we said in Section (15.2.2), if P grows slightly (logarithmically) faster than s, $A_I^*A_I$ is close to Id_s (see Talagrand inequality (15.1)), so that

$$\|p_F\|^2 \sim \|s_{0,I}\|^2 = s \tag{15.6}$$

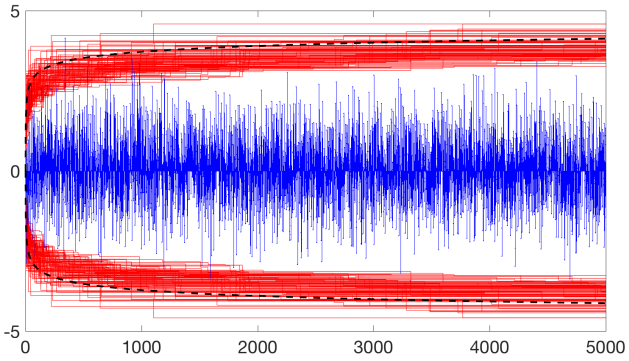

Figure 15.4: Graphical display of how the maximum of N i.i.d. gaussians concentrates tightly just bellow the $\sqrt{2\log(N)}$ dashed curve.

For a *fixed* p_F, one has that $\langle a_j, p_F \rangle$ is Gaussian distributed with variance $\|p_F\|^2/P$, and we use the well known fact (already encountered for denoising using thresholding) that the maximum of $P-s$ such vectors concentrates just bellow the universal threshold $\|p_F\|\sqrt{2\log(N-s)/P}$. Using the estimate (15.6), one sees that $\|p_F\|_\infty \leqslant 1$ is implied by $2\log(N)s/P \leqslant 1$, which gives the sharp scaling $P \geqslant 2\log(N)s$.

In order to get robustness to noise, one needs to impose that $\|A_{I^c}^* p_F\| < 1$, which can be achieve by using a slightly stronger scaling $P \geqslant 2(1+\delta)\log(N)s$ for a small δ.

One can actually make this reasoning very precise, because quite surprisingly, it turns out that $Ps/\|p_F\|^2$ is actually distributed according to a χ^2 variable with $P-s+1$ degrees of freedom (i.e. the sum of $P-s+1$ squares of Gaussian variables). Indeed, for $s=1$, one immediately sees that $P/\|p_F\|^2$ is χ^2 with P degrees of freedom. The general case is more involved, and the proof relies on the fact that the isotropy of the distribution implies that $p - P/\|p_F\|^2$ is the square of the distance between the first column of A_I and the linear space spanned by the other columns (hence $P-s+1$ degrees of freedom). Since one has a very good understanding of the clustering of such a χ^2 variable around its means, one can thus show that $\|p_F\| \leqslant (1-\delta)\sqrt{s}$ with high precision for arbitrary small $\delta > 0$. □

For $(N,s) \to +\infty$, one has $\delta \to 0$, so that informally, the scaling is

$$P \geqslant 2s\log(2N/\varepsilon). \tag{15.7}$$

This theorem states a non-uniform recovery guarantee, in the sense that one first choose a vector x_0, then draws the matrix A, and the recovery results holds with high probability. This should be contrasted with the RIP theory developed in Section 15.3 which provides stronger uniform guarantees.

15.3 RIP Theory for Uniform Guarantees

15.3.1 RIP Constants

The RIP constant δ_s of a matrix $\Phi \in \mathbb{R}^{P\times N}$ is defined as

$$\forall\, z \in \mathbb{R}^N, \quad \|z\|_0 \leqslant s \quad \Longrightarrow \quad (1-\delta_s)\|z\|^2 \leqslant \|\Phi z\|^2 \leqslant (1+\delta_s)\|z\|^2 \tag{15.8}$$

The following theorem states that for a sub-Gaussian random matrix, these RIP constant grows slowly with s. Let us stress that, although this is an abuse of notation, here we assume that A is a random matrix, and not a deterministic one as previously considered.

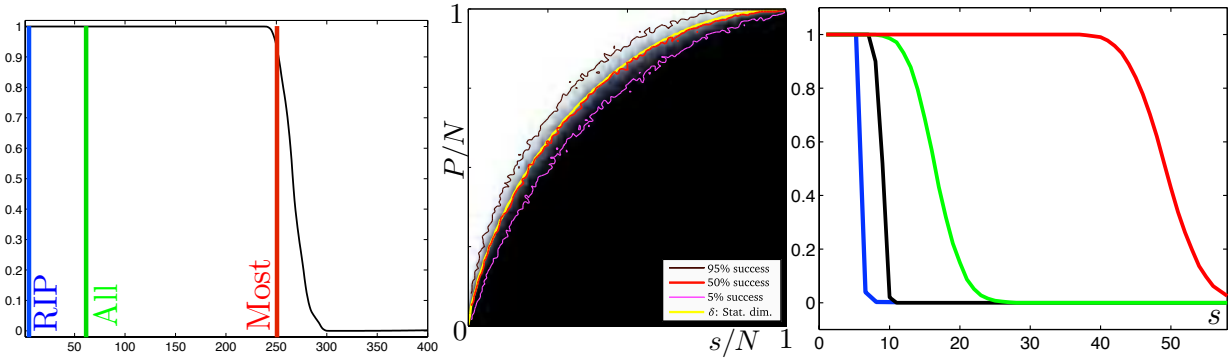

Figure 15.5: Phase transitions. For the figure on the right shows probability as function of sparsity that certain criteria hold true, blue: w-ERC, black: ERC, green $|\eta_F| \leqslant 1$, red: identifiability.

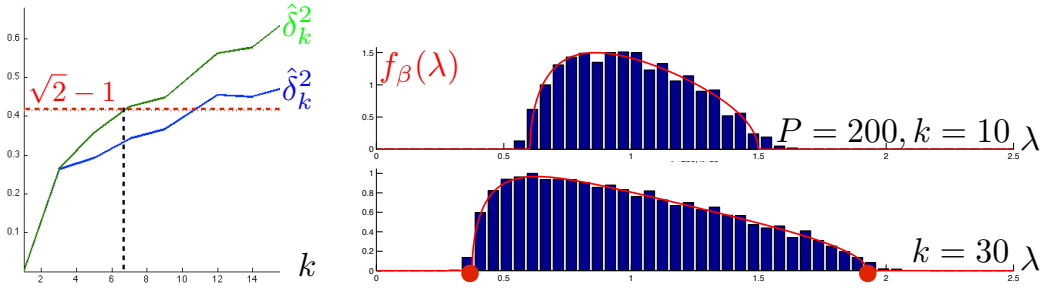

Figure 15.6: Left: evolution of lower bounds $\hat{\delta}_k$ on the RIP constant. Right: empirical distribution of singular values of Gaussian matrices.

Theorem 46. *If A is a sub-Gaussian random matrix, then provided*

$$P \geqslant C\delta^{-2} s \ln(eN/s) \tag{15.9}$$

it satisfies $\delta_s \leqslant 1$ with probability $1 - 2e^{-\delta^2 \frac{m}{2C}}$, where C only depends on the sub-Gaussianity parameters appearing in (22).

We do not prove this Theorem, and simply give the main intuition. The proof of this theorem relies on results regarding the distribution of the singular values of Gaussian matrices. Indeed, the RIP condition (15.8) is equivalent to having the bound $\mathrm{eig}(A_I^* A_I) \subset [1-\delta_s, 1+\delta_s]$ for all Gaussian matrices A_I extracted from A. In the Gaussian case (actually this holds for any random matrix with i.i.d. entries and unit covariance), one has a very good understanding of the distribution of the singular values of covariance matrices $B^* B \in \mathbb{R}^{s \times s}$ of a Gaussian matrix B of size (P, s), $B \sim \texttt{randn}(P, s)/\sqrt{P}$, as detailed in Section 15.2.2. In particular, using Talagrand concentration inequality (15.1), one obtains the desired controls over the δ_s constants.

15.3.2 RIP implies stable recovery

In the following, we fixe a vector $x \in \mathbb{R}^N$ and denote $y = \Phi x + w$ the measurement, with $\|w\| \leqslant \varepsilon$. We denote $\bar{x}_s \in \mathbb{R}^N$ the best s-term approximation of x, obtained by only keeping the s largest coefficients in magnitude from x and setting the others to 0.

We consider a solution $x^\star$ of

$$\min_{\|\Phi \tilde{x} - y\| \leqslant \varepsilon} \|\tilde{x}\|_1.$$

This note recall the proof from [7] of the following theorem

Theorem 47 ([7])**.** *If $\delta_{2s} \leqslant \sqrt{2} - 1$ then there exists C_0, C_1 such that*

$$\|x^\star - x_0\|_1 \leqslant \frac{C_0}{\sqrt{s}} \|\bar{x}_s - x_0\| + C_1 \varepsilon.$$

Putting together Theorems 46 and 47 gives the following recovery guarantee.

Theorem 48. *If A is a sub-Gaussian random matrix, then provided*

$$P \geqslant C\delta^{-2} s \ln(eN/s) \tag{15.10}$$

with probability $1 - 2e^{-\delta^2 \frac{P}{2C}}$ on the draw of A, one has that for every s-sparse signal,

$$\|x^\star - x_0\|_1 \leqslant \frac{C_0}{\sqrt{s}} \|x_s - x_0\| + C_1 \varepsilon.$$

In particular, if $\|w\| = 0$ and x_0 is s-sparse, setting $\varepsilon = 0$, one has $x^\star = x_0$.

This theorem provides a uniform recovery guarantee, in the sense that it means

$$\mathbb{P}(\forall\, s - \text{sparse } x_0, x^\star = x_0) \text{ goes fast to 1 when } P \to +\infty.$$

In contrast, theorem 45 proves a weaker non-uniform guarantee, in the sense that it means

$$\forall\, s - \text{sparse } x_0, \mathbb{P}(x^\star = x_0) \text{ goes fast to 1 when } P \to +\infty.$$

The recovery performance analysis based on RIP constants proves a better scaling in term of log-factors. This is because the analysis using η_F does not only imply stable recovery, it also provides stability of the support (sparsistency). Note however that the constants involved in the RIP analysis are very large (of the order of a few hundreds, as highlighted by Figure 15.6, left, and by Figure 15.5, right), while the constant appearing in (15.7) are small and known to be sharp.

Also, one can show that having small enough RIP constant implies the existence of a valid dual certificate (but this certificate is not necessarily η_F).

The remaining of this section is devoted to proving Theorem 47.

Notations. We denote x in place of x_0 and x_s in place of $\bar{x}_s$. We denote in the following $h = x^\star - x$ and denote T_0 the largest s coefficients of x in magnitude (so that $x_s = x_{T_0}$), T_1 the s largest coefficients of $h_{T_0^c}$, T_2 the following s largest coefficients of $h_{T_0^c}$ and so on. We denote $T = T_0 \cup T_1$ which is an index set of size $2s$.

Lemma 5. *One has*

$$\sum_{j \geqslant 2} \|h_{T_j}\| \leqslant \frac{1}{\sqrt{s}} \|h_{T_0^c}\|_1$$

Proof. By the definition of T_j for $j \geqslant 2$, one has, for all $j \geqslant 2$

$$\forall\, i \in T_{j-1}, \quad \|h_{T_j}\|_\infty \leqslant h_i,$$

and hence

$$\|h_{T_j}\|_\infty \leqslant \frac{1}{s} \|h_{T_{j-1}}\|_1.$$

This proves that

$$\|h_{T_j}\| \leqslant \sqrt{s} \|h_{T_j}\|_\infty \leqslant \frac{1}{\sqrt{s}} \|h_{T_{j-1}}\|_1$$

and thus

$$\sum_{j \geqslant 2} \|h_{T_j}\| \leqslant \frac{1}{\sqrt{s}} \sum_{j \geqslant 1} \|h_{T_j}\|_1 = \frac{1}{\sqrt{s}} \|h_{T_0^c}\|_1.$$

□

Lemma 6. *One has*

$$\|h_{T_0^c}\|_1 \leqslant \|h_{T_0}\|_1 + 2\|x_{T_0^c}\|_1$$

Proof. One has

$$\begin{aligned}
\|x\|_1 &\geqslant \|x + h\| && \text{because } x^\star \text{ is a minimizer} \\
&= \|(x+h)_{T_0}\|_1 + \|(x+h)_{T_0^c}\|_1 \\
&\geqslant \|x_{T_0}\|_1 - \|h_{T_0}\|_1 + \|h_{T_0^c}\|_1 - \|x_{T_0^c}\|_1 && \text{using the triangular inequality.}
\end{aligned}$$

Decomposing the left hand size $\|x\|_1 = \|x_{T_0}\|_1 + \|x_{T_0^c}\|_1$, one obtains the result. □

Lemma 7. *If z and z' have disjoints supports and $\|z\| \leqslant s$ and $\|z'\|_0 \leqslant s$,*

$$|\langle \Phi z,\, \Phi z' \rangle| \leqslant \delta_{2s} \|z\| \|z'\|.$$

Proof. Using the RIP (15.8) since $z \pm z'$ has support of size $2s$ and the fact that $\|z \pm z'\|^2 = \|z\|^2 + \|z'\|^2$, one has

$$(1 - \delta_{2s}) \left(\|z\|^2 + \|z'\|^2 \right) \leqslant \|\Phi z \pm \Phi z'\|^2 \leqslant (1 + \delta_{2s}) \left(\|z\|^2 + \|z'\|^2 \right).$$

One thus has using the parallelogram equality

$$|\langle \Phi z,\, \Phi z' \rangle| = \frac{1}{4} |\|\Phi z + \Phi z'\|^2 - \|\Phi z - \Phi z'\|^2|^2 \leqslant \delta_{2s} \|z\| \|z'\|.$$

□

Theorem 47 requires bounding $\|h\|$. We bound separately $\|h_T\|$ and $\|h_{T^c}\|$.

Part 1: bounding $\|h_T\|$. One has

$$\begin{aligned}
\|h_{T^c}\| = \|\sum_{j\geqslant 2} h_{T_j}\| &\leqslant \sum_{j\geqslant 2}\|h_{T_j}\| && \text{using the triangular inequality}\\
&\leqslant \frac{1}{\sqrt{s}}\|h_{T_0^c}\|_1 && \text{using Lemma 5}\\
&\leqslant \frac{1}{\sqrt{s}}\|h_{T_0}\|_1 + \frac{2}{\sqrt{s}}\|x_{T_0^c}\|_1 && \text{using Lemma 6}\\
&\leqslant \frac{1}{\sqrt{s}}\|h_{T_0}\|_1 + 2e_0 && \text{denoting } e_0 = \frac{1}{\sqrt{s}}\|x_{T_0^c}\|_1\\
&\leqslant \|h_{T_0}\| + 2e_0 && \text{using Cauchy-Schwartz}\\
&\leqslant \|h_T\| + 2e_0 && \text{because } T_0 \subset T.
\end{aligned}$$

The final bound reads

$$\|h_{T^c}\| \leqslant \|h_T\| + 2e_0. \tag{15.11}$$

Part 2: bounding $\|h_{T^c}\|$. One has

$$\begin{aligned}
\|h_T\|^2 &\leqslant \frac{1}{1-\delta_{2s}}\|\Phi h_T\|^2 && \text{using the RIP (15.8)}\\
&= \frac{A-B}{1-\delta_{2s}} && \text{using } \Phi h_T = \Phi h - \sum_{j\geqslant 2}\Phi h_{T_j},
\end{aligned}$$

where we have introduced

$$A = \langle \Phi h_T,\, \Phi h\rangle \quad \text{and} \quad B = \langle \Phi h_T,\, \sum_{j\geqslant 2}\Phi h_{T_j}\rangle.$$

One has

$$\begin{aligned}
|A| &\leqslant \|\Phi h_T\|\|\Phi h\| && \text{using Cauchy-Schwartz}\\
&\leqslant \sqrt{1+\delta_{2s}}\|h_T\|\|\Phi h\| && \text{using the RIP (15.8)}\\
&\leqslant \sqrt{1+\delta_{2s}}\|h_T\| 2\varepsilon && \text{using } \|\Phi h\| \leqslant \|\Phi x - y\| + \|\Phi x^\star - y\| \leqslant 2\varepsilon
\end{aligned}$$

The final bound reads

$$|A| \leqslant 2\varepsilon\sqrt{1+\delta_{2s}}\|h_T\| \tag{15.12}$$

One has

$$\begin{aligned}
|B| &\leqslant |\langle \Phi h_{T_0}, \sum_{j\geqslant 2}\Phi h_{T_j}\rangle| + |\langle \Phi h_{T_1}, \sum_{j\geqslant 2}\Phi h_{T_j}\rangle| && \text{using the triangular inequality}\\
&\leqslant \sum_{j\geqslant 2} |\langle \Phi h_{T_0}, \Phi h_{T_j}\rangle| + |\langle \Phi h_{T_0}, \Phi h_{T_j}\rangle| && \text{using the triangular inequality}\\
&\leqslant \sum_{j\geqslant 2} \delta_{2s}\|h_{T_0}\|\|h_{T_j}\| + \delta_{2s}\|h_{T_1}\|\|h_{T_j}\| && \text{using Lemma 7}\\
&= \delta_{2s}(\|h_{T_0}\| + \|h_{T_1}\|)\sum_{j\geqslant 2}\|h_{T_j}\|\\
&\leqslant \delta_{2s}\sqrt{2}\|h_T\|\sum_{j\geqslant 2}\|h_{T_j}\| && T_0 \text{ and } T_1 \text{ are disjoints}\\
&\leqslant \frac{\sqrt{2}\ \delta_{2s}}{\sqrt{s}}\|h_T\|\|h_{T_0^c}\|_1 && \text{using Lemma 5}
\end{aligned}$$

The final bound reads

$$|B| \leqslant \frac{\sqrt{2}\ \delta_{2s}}{\sqrt{s}} \|h_T\| \|h_{T_0^c}\|_1. \tag{15.13}$$

Putting together (15.12) and (15.13) one obtains

$$\|h_T\|^2 \leqslant \frac{\|h_T\|}{1-\delta_{2s}} \left(\sqrt{1+\delta_{2s}} 2\varepsilon + \frac{2}{\sqrt{s}} \delta_{2s} \|h_{T_0^c}\|_1 \right)$$

thus

$$\begin{aligned}
\|h_T\| &\leqslant \alpha\varepsilon + \frac{\rho}{\sqrt{s}} \|h_{T_0^c}\|_1 && \text{denoting} \begin{cases} \alpha = 2\frac{\sqrt{1+\delta_{2s}}}{1-\delta_{2s}}, \\ \rho = \frac{\sqrt{2}\delta_{2s}}{1-\delta_{2s}}. \end{cases} \\
&\leqslant \alpha\varepsilon + \frac{\rho}{\sqrt{s}} \|h_{T_0}\|_1 + \frac{2\rho}{\sqrt{s}} \|x_{T_0^c}\|_1 && \text{using Lemma 6} \\
&\leqslant \alpha\varepsilon + \rho \|h_{T_0}\| + 2\rho e_0 && \text{using Cauchy-Schwartz} \\
&\leqslant \alpha\varepsilon + \rho \|h_T\| + 2\rho e_0 && \text{because } T_0 \subset T.
\end{aligned}$$

Note that since $\delta_{2s} < \sqrt{2}-1$, one has $\rho < 1$. This implies

$$\|h_T\| \leqslant \frac{\alpha}{1-\rho}\varepsilon + \frac{2\rho}{1-\rho} e_0. \tag{15.14}$$

Conclusion. One has

$$\begin{aligned}
\|h\| &\leqslant \|h_T\| + \|h_{T^c}\| && \text{using the triangular inequality} \\
&\leqslant 2\|h_T\| + 2e_0 && \text{using (15.11)} \\
&\leqslant \frac{2\alpha}{1-\rho}\varepsilon + 2\frac{1+\rho}{1-\rho} e_0 && \text{using (15.14)}
\end{aligned}$$

which proves the theorem.

15.3.3 Fourier sampling RIP

A practical issue is that doing hardware implementing random operators A is very difficult, specially if this operator is "fully" random, i.e. if its entries are i.i.d. A more practical option is to use structured sampling operator, which are in some sense "less random". A possibility is to consider a random sub-sampling of orthogonal projection of the signal in some ortho-basis $\Xi = (\xi_\omega)_{\omega=1}^N$ of $\mathbb{R}^N$, so that

$$Ax \overset{\text{def.}}{=} (\langle x, \xi_\omega \rangle)_{\omega \in \Omega} \in \mathbb{R}^P \tag{15.15}$$

where $\Omega \subset \{1, \ldots, N\}$ is drawn uniformly at random among all sets of size P. The following theorem ensure that such an operator satisfies the RIP properties for large s (proportional to P up to log factors) is the atomes φ_ω are "spread enough", i.e. have a small magnitude, as measured by

$$\rho(\Xi) \overset{\text{def.}}{=} \sqrt{N} \max_{1 \leqslant \omega \leqslant N} \|\xi_\omega\|_\infty.$$

Theorem 49 (Rudelson-Vershinyn). *For any $0 < c < 1$, there exists C, such that provided that*

$$P \geqslant C\rho(\Xi)^2 s \log(N)^4 \tag{15.16}$$

with high probability on Ω, then A defined as in (15.15) satisfies $\delta_{2s} \leqslant c$.

One always has $1 \leqslant \rho(\Xi)^2 \leqslant N$. The worse case is ξ_ω to be Sirac atoms (i.e. $\Xi = \mathrm{Id}_N$), having $\rho(\Xi)^2 = N$, in which case P needs to be as large as N. In sharp contrast, optimal sampling bases are for instance Fourier atoms $\xi_\omega = (e^{\frac{2\mathrm{i}\pi}{N}\omega n})_{n=1}^N \in \mathbb{C}^N$, for which $\rho(\Xi) = 1$ (it is also possible to consider a Hadamard basis for instance). In this case, up to log-factors, the scaling (15.16) is similar to the one for sub-Gaussian matrices (15.10).

Theorem 49 deals with cases where the data x_0 to recover is sparse in the Dirac basis. If the data f_0 is sparse in another basis $\Psi = (\psi_m)_{m=1}^N$, one can do a change of variable $x = \Psi^* f$ (x being the coefficients of f in the basis Ψ), in which case $\rho(\Xi)$ appearing in (15.16) should be replaced by the mutual coherence between the sampling and the sparsity bases

$$\rho(\Psi^*\Xi) \overset{\text{def.}}{=} \sqrt{N} \max_{1\leqslant\omega,m\leqslant N} |\langle \psi_m, \xi_\omega \rangle|.$$

Good recovery performances are thus reached by (sampling,sparsity) pairs which are incoherent. The (Fourier,Dirac) pair is maximally incoherent. In contrast, Wavelet and Fourier are highly coherent. There exists explicit construction of "noiselets" bases which are almost maximally incoherent with wavelets. Note however that in contrast to Gaussian matrices, these structured measurement matrices are not universal, in the sense that there compressed sensing recovery performances depend on the sparsity basis Ψ which is used.

Bibliography

[1] P. Alliez and C. Gotsman. Recent advances in compression of 3d meshes. In N. A. Dodgson, M. S. Floater, and M. A. Sabin, editors, *Advances in multiresolution for geometric modelling*, pages 3–26. Springer Verlag, 2005.

[2] P. Alliez, G. Ucelli, C. Gotsman, and M. Attene. Recent advances in remeshing of surfaces. In *AIM@SHAPE repport*. 2005.

[3] Amir Beck. *Introduction to Nonlinear Optimization: Theory, Algorithms, and Applications with MATLAB*. SIAM, 2014.

[4] Stephen Boyd, Neal Parikh, Eric Chu, Borja Peleato, and Jonathan Eckstein. Distributed optimization and statistical learning via the alternating direction method of multipliers. *Foundations and Trends® in Machine Learning*, 3(1):1–122, 2011.

[5] Stephen Boyd and Lieven Vandenberghe. *Convex optimization*. Cambridge university press, 2004.

[6] E. Candès and D. Donoho. New tight frames of curvelets and optimal representations of objects with piecewise C^2 singularities. *Commun. on Pure and Appl. Math.*, 57(2):219–266, 2004.

[7] E. J. Candès. The restricted isometry property and its implications for compressed sensing. *Compte Rendus de l'Académie des Sciences*, Serie I(346):589–592, 2006.

[8] E. J. Candès, L. Demanet, D. L. Donoho, and L. Ying. Fast discrete curvelet transforms. *SIAM Multiscale Modeling and Simulation*, 5:861–899, 2005.

[9] A. Chambolle. An algorithm for total variation minimization and applications. *J. Math. Imaging Vis.*, 20:89–97, 2004.

[10] Antonin Chambolle, Vicent Caselles, Daniel Cremers, Matteo Novaga, and Thomas Pock. An introduction to total variation for image analysis. *Theoretical foundations and numerical methods for sparse recovery*, 9(263-340):227, 2010.

[11] Antonin Chambolle and Thomas Pock. An introduction to continuous optimization for imaging. *Acta Numerica*, 25:161–319, 2016.

[12] S.S. Chen, D.L. Donoho, and M.A. Saunders. Atomic decomposition by basis pursuit. *SIAM Journal on Scientific Computing*, 20(1):33–61, 1999.

[13] F. R. K. Chung. Spectral graph theory. *Regional Conference Series in Mathematics, American Mathematical Society*, 92:1–212, 1997.

[14] Philippe G Ciarlet. Introduction à l'analyse numérique matricielle et à l'optimisation. 1982.

[15] P. L. Combettes and V. R. Wajs. Signal recovery by proximal forward-backward splitting. *SIAM Multiscale Modeling and Simulation*, 4(4), 2005.

[16] P. Schroeder et al. D. Zorin. Subdivision surfaces in character animation. In *Course notes at SIGGRAPH 2000*, July 2000.

[17] I. Daubechies, M. Defrise, and C. De Mol. An iterative thresholding algorithm for linear inverse problems with a sparsity constraint. *Commun. on Pure and Appl. Math.*, 57:1413–1541, 2004.

[18] I. Daubechies and W. Sweldens. Factoring wavelet transforms into lifting steps. *J. Fourier Anal. Appl.*, 4(3):245–267, 1998.

[19] D. Donoho and I. Johnstone. Ideal spatial adaptation via wavelet shrinkage. *Biometrika*, 81:425–455, Dec 1994.

[20] Heinz Werner Engl, Martin Hanke, and Andreas Neubauer. *Regularization of inverse problems*, volume 375. Springer Science & Business Media, 1996.

[21] M. Figueiredo and R. Nowak. An EM Algorithm for Wavelet-Based Image Restoration. *IEEE Trans. Image Proc.*, 12(8):906–916, 2003.

[22] M. S. Floater and K. Hormann. Surface parameterization: a tutorial and survey. In N. A. Dodgson, M. S. Floater, and M. A. Sabin, editors, *Advances in multiresolution for geometric modelling*, pages 157–186. Springer Verlag, 2005.

[23] Simon Foucart and Holger Rauhut. *A mathematical introduction to compressive sensing*, volume 1. Birkhäuser Basel, 2013.

[24] I. Guskov, W. Sweldens, and P. Schröder. Multiresolution signal processing for meshes. In Alyn Rockwood, editor, *Proceedings of the Conference on Computer Graphics (Siggraph99)*, pages 325–334. ACM Press, August8–13 1999.

[25] A. Khodakovsky, P. Schröder, and W. Sweldens. Progressive geometry compression. In *Proceedings of the Computer Graphics Conference 2000 (SIGGRAPH-00)*, pages 271–278, New York, July 23–28 2000. ACMPress.

[26] L. Kobbelt. $\sqrt{3}$ subdivision. In Sheila Hoffmeyer, editor, *Proc. of SIGGRAPH'00*, pages 103–112, New York, July 23–28 2000. ACMPress.

[27] M. Lounsbery, T. D. DeRose, and J. Warren. Multiresolution analysis for surfaces of arbitrary topological type. *ACM Trans. Graph.*, 16(1):34–73, 1997.

[28] S. Mallat. *A Wavelet Tour of Signal Processing, 3rd edition.* Academic Press, San Diego, 2009.

[29] Stephane Mallat. *A wavelet tour of signal processing: the sparse way.* Academic press, 2008.

[30] D. Mumford and J. Shah. Optimal approximation by piecewise smooth functions and associated variational problems. *Commun. on Pure and Appl. Math.*, 42:577–685, 1989.

[31] Neal Parikh, Stephen Boyd, et al. Proximal algorithms. *Foundations and Trends® in Optimization*, 1(3):127–239, 2014.

[32] Gabriel Peyré. *L'algèbre discrète de la transformée de Fourier.* Ellipses, 2004.

[33] Gabriel Peyré and Marco Cuturi. Computational optimal transport. 2017.

[34] J. Portilla, V. Strela, M.J. Wainwright, and Simoncelli E.P. Image denoising using scale mixtures of Gaussians in the wavelet domain. *IEEE Trans. Image Proc.*, 12(11):1338–1351, November 2003.

[35] E. Praun and H. Hoppe. Spherical parametrization and remeshing. *ACM Transactions on Graphics*, 22(3):340–349, July 2003.

[36] L. I. Rudin, S. Osher, and E. Fatemi. Nonlinear total variation based noise removal algorithms. *Phys. D*, 60(1-4):259–268, 1992.

[37] Filippo Santambrogio. Optimal transport for applied mathematicians. *Birkäuser, NY*, 2015.

[38] Otmar Scherzer, Markus Grasmair, Harald Grossauer, Markus Haltmeier, Frank Lenzen, and L Sirovich. *Variational methods in imaging*. Springer, 2009.

[39] P. Schröder and W. Sweldens. Spherical Wavelets: Efficiently Representing Functions on the Sphere. In *Proc. of SIGGRAPH 95*, pages 161–172, 1995.

[40] P. Schröder and W. Sweldens. Spherical wavelets: Texture processing. In P. Hanrahan and W. Purgathofer, editors, *Rendering Techniques '95*. Springer Verlag, Wien, New York, August 1995.

[41] C. E. Shannon. A mathematical theory of communication. *The Bell System Technical Journal*, 27(3):379–423, 1948.

[42] A. Sheffer, E. Praun, and K. Rose. Mesh parameterization methods and their applications. *Found. Trends. Comput. Graph. Vis.*, 2(2):105–171, 2006.

[43] Jean-Luc Starck, Fionn Murtagh, and Jalal Fadili. *Sparse image and signal processing: Wavelets and related geometric multiscale analysis*. Cambridge university press, 2015.

[44] W. Sweldens. The lifting scheme: A custom-design construction of biorthogonal wavelets. *Applied and Computation Harmonic Analysis*, 3(2):186–200, 1996.

[45] W. Sweldens. The lifting scheme: A construction of second generation wavelets. *SIAM J. Math. Anal.*, 29(2):511–546, 1997.